Scalings for Submarine Melting at Tidewater Glaciers from Buoyant Plume Theory

Scalings for Submarine Melting at Tidewater Glaciers from Buoyant Plume Theory

DONALD A. SLATER, DAN N. GOLDBERG, PETER W. NIENOW, AND TOM R. COWTON

School of Geosciences, University of Edinburgh, Edinburgh, United Kingdom

(Manuscript received 14 July 2015, in final form 12 March 2016)

ABSTRACT

Rapid dynamic changes at the margins of the Greenland Ice Sheet, synchronous with ocean warming, have raised concern that tidewater glaciers can respond sensitively to ocean forcing. Understanding of the processes encompassing ocean forcing nevertheless remains embryonic. The authors use buoyant plume theory to study the dynamics of proglacial discharge plumes arising from the emergence of subglacial discharge into a fjord at the grounding line of a tidewater glacier, deriving scalings for the induced submarine melting. Focusing on the parameter space relevant for high discharge tidewater glaciers, the authors suggest that in an unstratified fjord the often-quoted relationship between total submarine melt volume and subglacial discharge raised to the $^1/_3$ power is appropriate regardless of plume geometry, provided discharge lies below a critical value. In these cases it is then possible to formulate a simple equation estimating total submarine melt volume as a function of discharge, fjord temperature, and calving front height. However, once linear stratification is introduced—as may be more relevant for fjords in Greenland—the total melt rate discharge exponent may be as large as $^3/_4$ ($^2/_3$) for a point (line) source plume and display more complexity. The scalings provide a guide for more advanced numerical models, inform understanding of the processes encompassing ocean forcing, and facilitate assessment of the variability in submarine melting both in recent decades and under projected atmospheric and oceanic warming.

1. Introduction

Loss of ice from the Greenland Ice Sheet contributed ~8 mm to global sea level between 1992 and 2012 (Shepherd et al. 2012; Vaughan et al. 2013), with the rate of loss accelerating over the same period (Rignot et al. 2011), such that between 2009 and 2012, Greenland contributed ~1 mm yr^{-1} to global sea level (Enderlin et al. 2014). Driven by a period of tidewater glacier acceleration and retreat (Moon et al. 2012; Jiskoot et al. 2012), ice flux into the ocean from tidewater glaciers accounted for approximately half of Greenland's mass balance deficit in the early 2000s (van den Broeke et al. 2009). Tidewater glacier dynamics can therefore have a significant impact on Greenland Ice Sheet mass balance.

The dramatic changes observed at many of Greenland's outlet glaciers occurred during a period of atmospheric and oceanic warming (Mernild et al. 2014; Rignot et al. 2012); however, a conclusive attribution of the response of tidewater glaciers to one of these factors remains elusive. Indeed, many of the processes affecting tidewater glaciers are promoted by both of these forcings, such that a full understanding of the dynamics likely requires consideration of both atmospheric and oceanic factors (Straneo and Cenedese 2015). One such process is submarine melting of the calving front, on which this paper is focused.

Submarine melting may contribute to mass loss either directly via melting of submerged ice (Motyka et al. 2013; Bartholomaus et al. 2013; Inall et al. 2014) or indirectly by controlling calving style and rate (O'Leary 2011; Chauché et al. 2014) or grounded ice flux (Holland et al. 2008). Submarine melting is thought to be promoted by both the presence of warm water of subtropical origin in

Denotes Open Access content.

Supplemental information related to this paper is available at the Journals Online website: http://dx.doi.org/10.1175/JPO-D-15-0132.s1.

Corresponding author address: Donald A. Slater, School of Geosciences, University of Edinburgh, Drummond Street, Edinburgh EH8 9XP, United Kingdom.
E-mail: d.slater@ed.ac.uk

DOI: 10.1175/JPO-D-15-0132.1

Greenlandic fjords (Straneo et al. 2010; Mortensen et al. 2011) and the emergence of subglacial discharge at the grounding line of the glacier (Jenkins 2011). Presence of the latter results in proglacial plumes as the discharge rises buoyantly, and the high ice-adjacent water velocities generated increase the turbulent transfer of heat to the ice. These proglacial plumes are the focus of this study.

Given the difficulties of directly measuring submarine melt rates, estimates have to date relied either on modeling or on hydrographic data taken some distance from the glacier terminus. The hydrographic data can in theory be used to calculate a net toward-glacier heat flux. This method has been applied around Greenland to obtain submarine melt rates ranging from 0.7 to 10 m day^{-1} (Rignot et al. 2010; Sutherland and Straneo 2012; Xu et al. 2012; Inall et al. 2014). Such estimates should, however, be viewed with caution, as fjord dynamics can display significant short-term variability (Jackson et al. 2014; Straneo and Cenedese 2015) such that a calculated melt rate may not be indicative of a longer-term mean. There may also be considerable loss of heat between the flux gate and calving front because of the melting of submerged proglacial ice mélange (Inall et al. 2014).

An alternative approach uses high-resolution numerical modeling to predict ice-adjacent water velocities and temperatures, which are then converted to a submarine melt rate using a melt parameterization (Holland and Jenkins 1999). This has been undertaken in both two (Xu et al. 2012; Sciascia et al. 2013, 2014) and three dimensions (Xu et al. 2013; Kimura et al. 2014; Slater et al. 2015; Carroll et al. 2015). These models have facilitated investigation of the spatial distribution of submarine melting and of how submarine melting responds to variations in subglacial discharge, fjord temperature, and near-terminus subglacial hydrology. A key result from these studies is that per plume, submarine melt rate responds sublinearly to increasing subglacial discharge. Specifically, these studies suggest a relation $\dot{m} \propto Q^{\gamma}$ between submarine melt rate $\dot{m}$ and subglacial discharge Q, with γ taking various values from $\gamma < 1/3$ (Kimura et al. 2014) to $1/3$ (Xu et al. 2012; Sciascia et al. 2013; Kimura et al. 2014), $1/2$ (Sciascia et al. 2013; Xu et al. 2013), and $\sim$0.85 (Xu et al. 2013). All studies show a linear response of melt rate to variation in water temperature (Sciascia et al. 2013; Xu et al. 2013). Finally, Slater et al. (2015) suggested that the total submarine melt volume is greater if the subglacial discharge emerges via drainage that is distributed across the grounding line rather than concentrated in a few large channels. Numerical models, however, rely on a melt parameterization that has as yet been validated only beneath an Antarctic ice shelf (Jenkins et al. 2010), which is likely a substantially different setting to vertical calving fronts at tidewater glaciers.

A final method of investigating submarine melt rates—and the approach taken in this study—is buoyant plume theory (BPT). BPT has been successfully applied to a wide range of environmental phenomena, traceable back to the classic paper by Morton et al. (1956). BPT describes the evolution of a source of buoyancy as it rises through an ambient fluid. In this glacial application we use BPT to describe ice-adjacent water velocity and temperature within a proglacial plume. This approach avoids recourse to computationally expensive numerical simulations but is limited to idealized geometries. BPT has previously been applied to tidewater glaciers. MacAyeal (1985) and Jenkins (1991) were pioneering papers on the glacial application of BPT. Wells and Worster (2008) developed the theoretical basis of coupling plume theory with submarine melting while Jenkins (2011) used BPT to propose, in advance of the numerical studies reported above, a cube root dependence of submarine melt rate on subglacial discharge and a linear dependence on fjord temperature. O'Leary (2011) applied BPT to obtain submarine melt rates for three glaciers in West Greenland, and Cenedese and Linden (2014) have used laboratory experiments to investigate plume dynamics with a glacial motivation. Most recently, Cowton et al. (2015) used BPT to force the glacier boundary of an ocean general circulation model adapted to a fjord and Carroll et al. (2015) employed BPT to investigate plume outflow depth in a fjord.

In spite of the increasing body of research on submarine melting, there remain significant gaps in our understanding, both observationally (there has yet to be a direct measurement of submarine melting at a tidewater glacier) and in the modeling (for example, the wide range of melt discharge exponent γ values present in the literature). Given the potential importance of submarine melting for tidewater glacier dynamics, there is a need for further investigation of ice–ocean interaction, of which this study is an example.

This study uses BPT to investigate the dynamics of plumes in contact with the vertical calving fronts of tidewater glaciers with a focus on the submarine melt induced by the plume. We investigate both point and line plume sources and consider a fjord that is uniformly or linearly stratified. We also explore under what conditions a plume will reach the fjord surface. In undertaking these investigations we aim to (i) explain the variation in the value of the melt discharge exponent

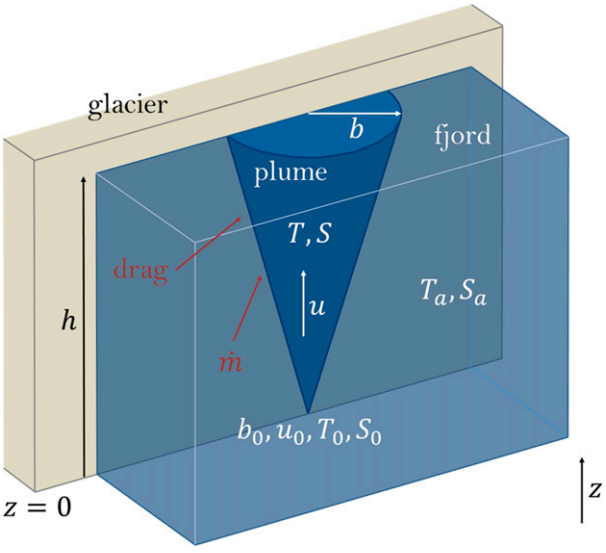

FIG. 1. The half-conical plume considered in this study. The plume emerges into the fjord at the grounding line of the glacier and rises buoyantly, growing through entrainment of ambient fjord water.

γ found in the literature, (ii) suggest under what conditions a certain melt exponent may apply, and (iii) facilitate assessment of the likely variation in submarine melt at tidewater glaciers, both in recent decades and under future climate scenarios.

2. Methods

a. Introduction to the model

In this paper we consider mainly a half-conical geometry for proglacial plumes (Fig. 1), which we believe to be appropriate for plumes arising from channelized subglacial drainage. The glacier terminates in a fjord of depth h and is assumed to have a vertical calving front in contact with the flat side of the plume. The plume has radius $b(z)$, vertical velocity $u(z)$, temperature $T(z)$, and salinity $S(z)$, assumed uniform across the radius of the plume. It experiences drag (coefficient C_d) and induces submarine melt $\dot{m}(z)$ where in contact with the ice. The proglacial fjord has temperature $T_a(z)$ and salinity $S_a(z)$, referred to as ambient conditions.

The plume is initiated at the glacier grounding line by a source of cold and fresh subglacial discharge. With a Greenlandic application in mind, the proglacial fjord is saline. Thus, the density $\rho(z)$ of the plume—defined through an equation of state as a function of its temperature and salinity—is initially less than that of the ambient water $\rho_a(z)$, and the plume rises buoyantly. We assume that the plume is turbulent at the source. Turbulence causes the plume to entrain ambient water so that it grows as it rises. Following Morton et al. (1956) and numerous other successful applications of BPT, we assume that the rate of entrainment into the plume is proportional to plume velocity u, with a constant of proportionality α.

The entrainment of ambient water means that the temperature and salinity (and therefore density) of the plume are diluted toward the ambient conditions, thereby altering the plume buoyancy. If as a result the plume density exceeds the ambient water density, the plume is then negatively buoyant, will slow down, and may not reach the fjord surface.

b. Defining equations

To quantify the evolution of the plume as it rises, we introduce a set of equations with the half-conical geometry modified from Morton et al. (1956) and the coupling to submarine melt by Jenkins (2011) (though the plume considered therein was a two-dimensional line plume). The equations have been previously applied by Cowton et al. (2015) and conserve the volume, momentum, heat, and salt flux of the plume, respectively:

$$\frac{d}{dz}\left(\frac{\pi}{2}b^2u\right) = \pi\alpha bu + 2b\dot{m}, \tag{1a}$$

$$\frac{d}{dz}\left(\frac{\pi}{2}b^2u^2\right) = \frac{\pi}{2}b^2g' - 2C_dbu^2, \tag{1b}$$

$$\frac{d}{dz}\left(\frac{\pi}{2}b^2uT\right) = \pi\alpha buT_a + 2b\dot{m}T_b - 2C_d^{1/2}\Gamma_T bu(T - T_b), \tag{1c}$$

and

$$\frac{d}{dz}\left(\frac{\pi}{2}b^2uS\right) = \pi\alpha buS_a + 2b\dot{m}S_b - 2C_d^{1/2}\Gamma_S bu(S - S_b), \tag{1d}$$

where $g' = g(\rho_a - \rho)/\rho_{\text{ref}}$ is the reduced gravity of the plume, denoted g'_0 when evaluated at the glacier grounding line; ρ_{ref} is a Boussinesq reference density; C_d is the drag coefficient; and Γ_T and Γ_S are heat and salt transfer coefficients. Submarine melt rate $\dot{m}$ and ice–ocean boundary temperature T_b and salinity S_b are defined by the three-equation melt formulation (Holland and Jenkins 1999):

$$\dot{m}[c_i(T_b - T_i) + L] = c_wC_d^{1/2}\Gamma_T u(T - T_b), \tag{2a}$$

$$\dot{m}S_b = C_d^{1/2}\Gamma_S u(S - S_b), \quad \text{and} \tag{2b}$$

$$T_b = \lambda_1S_b + \lambda_2 + \lambda_3(h - z). \tag{2c}$$

Here the values λ_i describe the variation of freezing point with salinity, constant offset, and variation with

depth; c_i and c_w are the heat capacities of ice and water; and T_i is ice temperature (ice salinity is zero).

With a nonlinear equation of state (e.g., Fofonoff and Millard 1983), Eqs. (1a)–(2c) are referred to in this paper as the full model (FM), the solution of which is achieved by numerical integration. To develop scalings for plume variables and submarine melt under variation in the inputs, we require the model to be analytically tractable, and we thus now describe some simplifications.

c. Analytical model

The first simplification is to neglect the feedback of submarine melting on the plume. This entails removing the last term on the right-hand side of Eq. (1a), representing the volume added by submarine melting, and the last two terms on the right hand sides of Eqs. (1c) and (1d), representing the cooling and freshening effect of submarine melting, and heat and salt transfer out of the plume to the ice–ocean interface. Thus, we are limiting ourselves to considering convection-driven melt rather than melt-driven convection; that is, we assume that the buoyancy provided by subglacial discharge dominates over the buoyancy added by submarine melting. It can be shown (see supplemental material) that for ambient water of temperature T_a and subglacial discharge Q_{0m} at temperature T_0, this is the case for length scales $z < Z_m$ above the grounding line, where Z_m is given by

$$Q_{0m}^{2/3} \approx \frac{c_w C_d^{1/2} \Gamma_T}{L} \left(\frac{9\alpha g_0'}{5\pi} \right)^{1/3} (T_a - T_0) Z_m^{5/3}. \qquad (3)$$

Equivalently, at a calving front of height Z_m, Eq. (3) gives the subglacial discharge Q_{0m}, above which we may neglect the melt feedback. For a calving front that is 500 m high and for a fjord with $T_a = 3$°C and $S_a = 34$ psu, we obtain $Q_{0m} \approx 0.2\,\mathrm{m^3\,s^{-1}}$. For the largest calving front considered in this study (900 m) and for the warmest water ($T_a = 6$°C), we obtain $Q_{0m} \approx 2\,\mathrm{m^3\,s^{-1}}$. In summary, a conservative estimate for the subglacial discharge below which submarine melting has an important feedback on the plume at real tidewater glaciers is $Q_{0m} \approx 5\,\mathrm{m^3\,s^{-1}}$; in many cases it will be somewhat smaller. Above this critical discharge, numerical results show that the melt feedback affects plume temperature by <2% and salinity by <0.5%. Note that our focus in this paper on discharges significantly larger than Q_{0m} is equivalent to focusing on length scales z satisfying $z \ll Z_m$. This marks an important difference with the paper of Jenkins (2011), which focused on a line plume in the region $z \sim Z_m$.

Further simplification is achieved by neglecting the plume-ice frictional drag that appears as the second term on the right-hand side of Eq. (1b); inclusion of this term reduces plume velocity by only ~2.5% in a uniform stratification (supplemental material). We also make use of a linear equation of state as in Jenkins (2011):

$$\rho = \rho_{\mathrm{ref}}[1 + \beta_S(S - S_{\mathrm{ref}}) - \beta_T(T - T_{\mathrm{ref}})]. \qquad (4)$$

The simplified system of equations, consisting of Eqs. (1a)–(1d) with only the first term on each of the right-hand sides, together with Eqs. (2a)–(2c) and the equation of state Eq. (4), will be referred to as the analytical model (AM).

d. Initial conditions

Solution of Eqs. (1a)–(1d) requires initial conditions for plume radius b_0, velocity u_0, temperature T_0, and salinity S_0. Since the plume is initiated by fresh subglacial discharge at the pressure melting point, we take $T_0 = \lambda_2 + \lambda_3 h$ and $S_0 = 0$ psu. It is less clear how to choose b_0 and u_0.

The simplicity of this model requires that the subglacial discharge emerges into the fjord vertically, a situation that is unlikely to occur at a tidewater glacier. Horizontal emergence may be more realistic, as the subglacial channel feeding the plume presumably lies along the ice–bed interface prior to reaching the grounding line. Horizontal emergence has been implemented in previous models, with choice of channel size and flow velocity based on the Manning equation (Mugford and Dowdeswell 2011) or balance of wall melt and creep closure (Slater et al. 2015). Numerical models suggest that discharge emerging horizontally quickly transitions to vertical flow, after which point our model should be applicable. We should therefore treat our results near the grounding line with caution.

One constraint on b_0 and u_0 is provided by specifying the subglacial discharge $Q_0 = \pi b_0^2 u_0/2$, but this does not uniquely fix b_0 and u_0; a discharge Q_0 can be achieved with a plume that is initially slow and wide, or one that is fast and narrow. These possibilities are distinguished by their ratio of buoyancy to momentum, a property quantified by a dimensionless number $\Gamma = 5bg'/8\alpha u^2$ (e.g., Morton 1959; Turner 1973; Kaye 2008). A plume with $\Gamma = 1$ is described as pure, having a balance of buoyancy and momentum. Choice of the source value Γ_0 provides a second constraint to uniquely fix b_0 and u_0. In a uniform stratification, a plume will quickly tend toward $\Gamma = 1$ as it rises (Hunt and Kaye 2005). The plume is therefore

quickly insensitive to the value of Γ_0, and we choose $\Gamma_0 = 1$ throughout this paper. Relaxing this assumption does not significantly affect our results, particularly when not close to the grounding line. Solving the two constraints provided by Q_0 and Γ_0, initial plume radius and velocity are given by

$$b_0 = \left(\frac{32\alpha\Gamma_0 Q_0^2}{5\pi^2 g_0'}\right)^{1/5} \quad \text{and} \quad u_0 = \frac{2}{\pi}\left(\frac{5\pi^2 g_0'}{32\alpha\Gamma_0}\right)^{2/5} Q_0^{1/5}, \tag{5}$$

where, as discussed above, we set $\Gamma_0 = 1$ unless stated otherwise.

To solve the model we now require only ambient conditions $T_a(z)$ and $S_a(z)$ and subglacial discharge Q_0. For two classes of ambient stratification (uniform and linear), we proceed with the analytical model to obtain fundamental scalings for plume properties and submarine melt under variation in the inputs. Values of the physical parameter values used are provided in Table S1.

3. Uniform stratification

a. Solution of defining equations

The simplest ambient conditions we can consider are those of a uniformly stratified fjord, where temperature and salinity do not vary with depth. This situation is relevant typically to proglacial fjords in Alaska (Bartholomaus et al. 2013) and also at depth in Greenland (Chauché et al. 2014). In addition plume dynamics in a uniform stratification provide a good approximation to the initial rise of a plume in a linear stratification (Morton 1959), and many of the results regarding submarine melting carry over to the linearly stratified case.

The solution to the analytical model in a uniform stratification (T_a, S_a), for a source of discharge Q_0, satisfying $T(0) = T_0$ and $S(0) = 0$ and with initial radius and velocity as defined in Eqs. (5), is (e.g., Morton et al. 1956; Turner 1973; Straneo and Cenedese 2015)

$$b = \frac{6}{5}\alpha(z + z_0), \quad u = \frac{5}{6\alpha}\left(\frac{9\alpha Q_0 g_0'}{5\pi}\right)^{1/3}(z + z_0)^{-1/3}, \quad \text{and} \tag{6a}$$

$$T = T_0 + (T_a - T_0)\left[1 - \left(\frac{z_0}{z + z_0}\right)^{5/3}\right],$$

$$S = S_a\left[1 - \left(\frac{z_0}{z + z_0}\right)^{5/3}\right], \tag{6b}$$

where

$$z_0 = \frac{5}{6\alpha}\left(\frac{32\alpha Q_0^2}{5\pi^2 g_0'}\right)^{1/5} \quad \text{and} \quad g_0' = g[\beta_S S_a - \beta_T(T_a - T_0)]. \tag{6c}$$

Some example solutions are plotted in Fig. 2. Note that this solution holds regardless of the sign of $T_a - T_0$, though we focus here on the $T_a > T_0$ case, which is not a significant restriction for vertical calving fronts. The solution in Eqs. (6), including the split of buoyancy into temperature and salinity, is now entirely specified by the four parameters Q_0, T_a, S_a, and h. Note that after setting $\Gamma_0 = 1$, z_0 is the one remaining independent characteristic length scale of the problem (e.g., Kaye 2008) and ranges between 0 and 100 m for Q_0 between 0 and 1000 $\mathrm{m^3\,s^{-1}}$. An established result (Morton 1959) is that a finite source pure plume (of which ours is an example since $Q_0 \neq 0$ and $\Gamma_0 = 1$) is equivalent to a plume emanating from a point source of buoyancy only situated a distance z_0 below the finite source. Furthermore, z_0 may be interpreted as the length scale over which the initial conditions influence plume dynamics (Morton 1959; Wright and Wallace 1979). Therefore, for $z \ll z_0$ (i.e., close to the grounding line) plume properties are dominated by the initial conditions while for $z \gg z_0$ (i.e., far from the grounding line, or the point source limit) the plume has "forgotten" its initial properties. In particular, z_0 provides the characteristic length scale that determines how quickly plume temperature and salinity approach ambient values.

b. Local submarine melt rates

Local submarine melt rates are calculated by substituting Eqs. (6a)–(6c) into Eqs. (2a)–(2c) and are plotted in Figs. 2e, 2j, and 2o. Immediately above the grounding line, melt increases quickly with height as the plume warms through entrainment of ambient water. Far from the grounding line, when plume temperature is close to the ambient, variation in melt with height is dominated by velocity and decays as the inverse cube root of distance above the virtual source. The maximum melt rate is located at depth between these two regions. We now discuss the effect of Q_0, T_a, and S_a on melt rates. Qualitatively, melt appears insensitive to S_a (Fig. 2e), linearly sensitive to T_a (Fig. 2j), and sublinearly sensitive to Q_0 (Fig. 2o).

Consider first the dependence of melt on S_a. Plume velocity is weakly affected and plume salinity responds approximately linearly to S_a [Eqs. (6) and Fig. 2]. The submarine melt parameterization does respond to change in plume salinity through S_b and T_b; however, percentage changes in S_a in glacial settings are typically small (e.g., Straneo and Cenedese

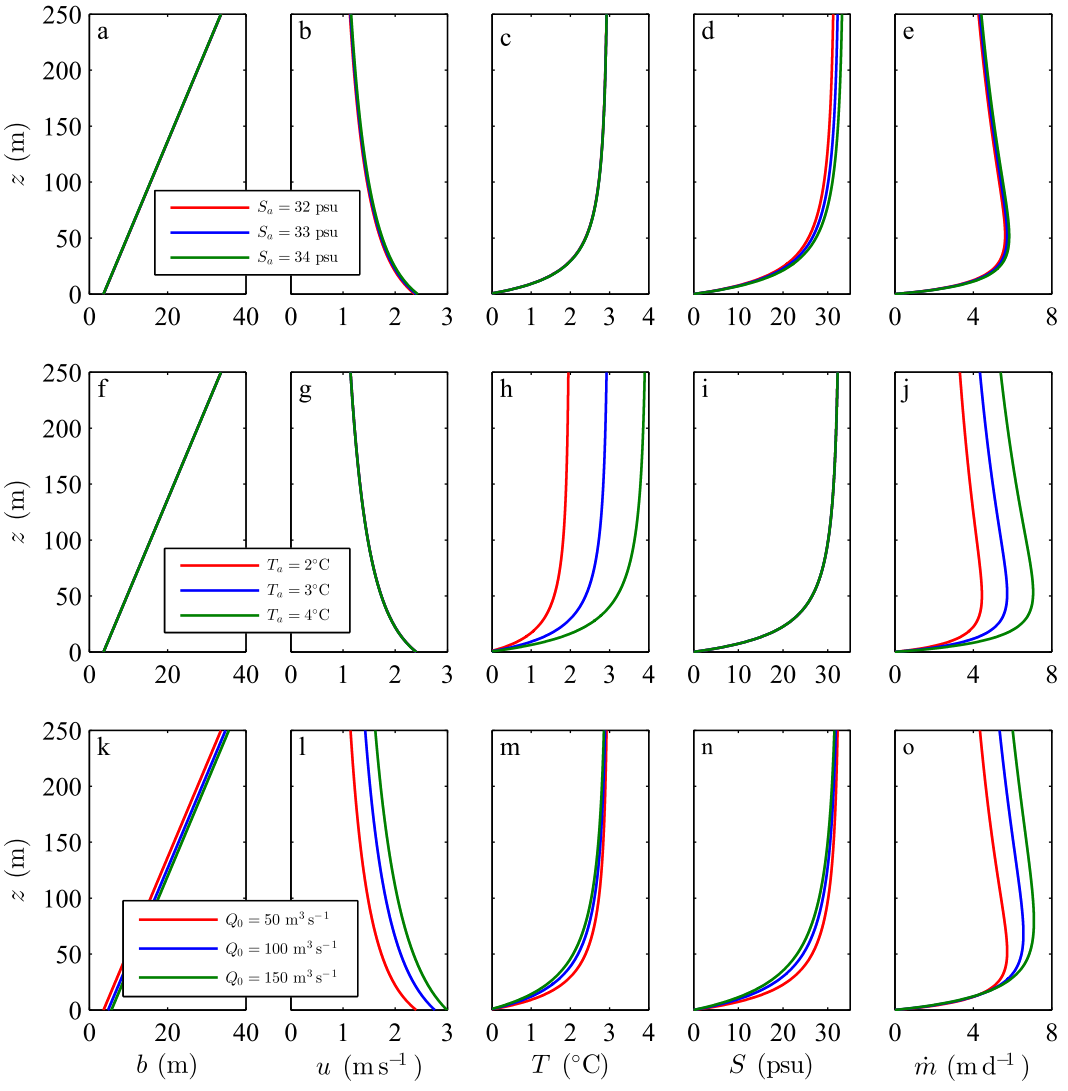

FIG. 2. Effect of change in (a)–(e) S_a, (f)–(j) T_a, and (k)–(o) Q_0 on the half-conical plume in a uniform stratification. Unless being varied, the forcing parameters take values $Q_0 = 50\ m^3\ s^{-1}$, $T_a = 3°C$, and $S_a = 33$ psu. Results shown are for the analytical model.

2015) and therefore do not result in significant variability in melt rates (Figs. 2e, 4d). Turning to the response of submarine melt rate to change in T_a, Eqs. (6) and Fig. 2 show that the only plume variable that responds significantly to T_a is plume temperature, and that it does so in an approximately linear fashion. The submarine melt parameterization is also close to linear in plume temperature (Holland and Jenkins 1999), and it therefore follows that melt rates respond linearly to T_a.

Sensitivity to subglacial discharge Q_0 is more complex. Previous studies (e.g., Jenkins 2011) have motivated a power-law relationship between local submarine melt rate and subglacial discharge, $\dot{m} \propto Q_0^{\gamma}$. Supposing γ were constant, we'd have $\gamma = (Q_0/\dot{m})d\dot{m}/dQ_0$; therefore, it is useful to consider

$$\frac{Q_0}{\dot{m}}\frac{d\dot{m}}{dQ_0} = \frac{Q_0}{u}\frac{du}{dQ_0} + \frac{Q_0}{T - T_b}\frac{d}{dQ_0}(T - T_b) \tag{7a}$$

$$= \frac{1}{3}\left(1 - \frac{2}{5}\frac{z_0}{z + z_0}\right) + \frac{Q_0}{T - T_b}\left[\frac{dT}{dQ_0}\left(1 - \frac{dT_b}{dT}\right) - \frac{dS}{dQ_0}\frac{dT_b}{dS} - \frac{du}{dQ_0}\frac{dT_b}{du}\right], \tag{7b}$$

where we have used the fact that $c_i(T_b - T_i) \ll L$ in Eq. (2a). Note that, in general, Eq. (7b) retains dependence on z and Q_0, and therefore there is no single value for γ that applies universally. Differentiation of Eq. (6b)

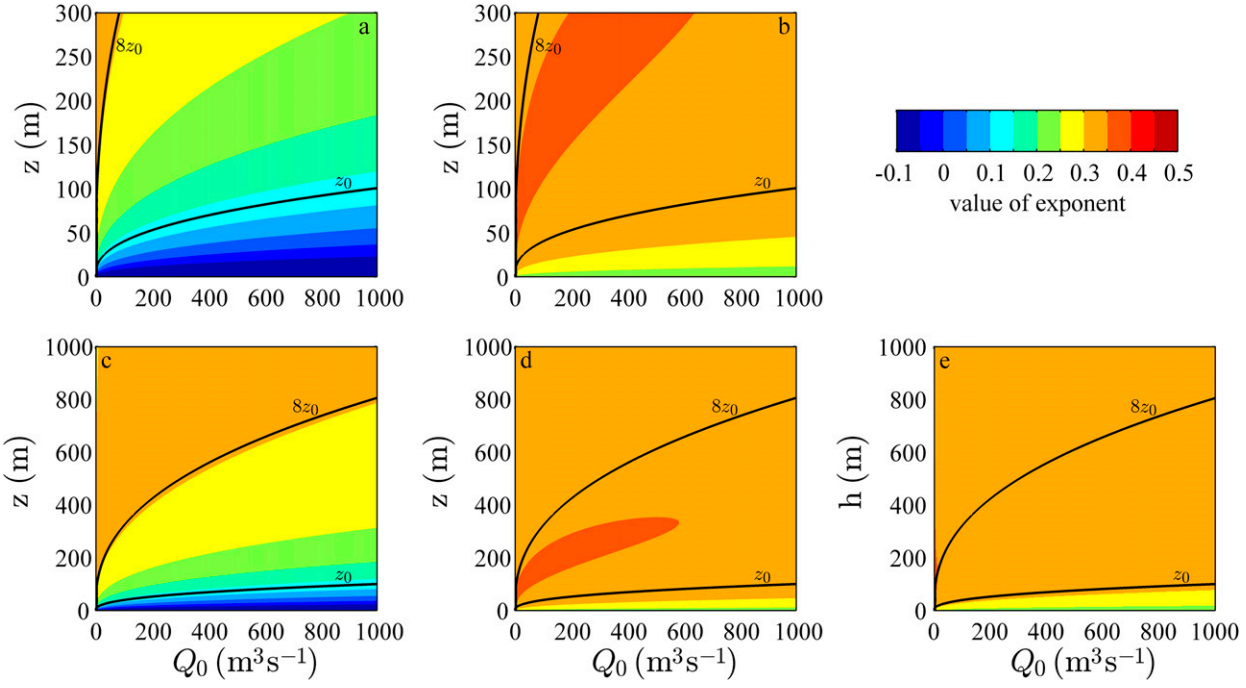

FIG. 3. (a),(c) Plots of local melt rate discharge exponent (i.e., γ in the relationship $\dot{m} \propto Q_0^{\gamma}$) as a function of subglacial discharge Q_0 and height above grounding line z. (b),(d) Exponent of the integrand in Eq. (9) (i.e., γ in the relationship $b\dot{m} \propto Q_0^{\gamma}$). Calving front height $h =$ 300 m in (a) and (b) and $h = 1000$ m in (c) and (d). Note that (a) and (b) are not quite zoomed-in versions of (c) and (d) because of the weak dependence of melt rate on pressure. (e) Total melt rate discharge exponent (i.e., γ in the relationship $\dot{M} \propto Q_0^{\gamma}$) as a function of Q_0 and h. Black lines show multiples of z_0. We take $T_a = 3°C$ and $S_a = 33$ psu throughout. Results are generated using the full model.

gives the response of plume temperature to change in subglacial discharge

$$\frac{dT}{dQ_0} = -\frac{2(T_a - T_0)}{3Q_0}\left(\frac{z_0}{z+z_0}\right)^{5/3}\frac{z}{z+z_0}, \qquad (8)$$

which, provided $T_a > T_0$, is always negative. This means that at a fixed depth, plume temperature decreases as initial flux increases. This arises because it takes longer to dilute the initial temperature through entrainment when there is a larger initial volume flux. A similar conclusion holds for dS/dQ_0.

We can use the melt rate parameterization Eqs. (2a)–(2c) to show that $dT_b/du = 0, 0 < dT_b/dT < 1$, and $dT_b/dS < 0$ (supplemental material). Therefore, if $T_a > T_0$, the second term on the right-hand side of Eq. (7a) is negative (i.e., the effect of increasing subglacial discharge on plume thermal forcing causes a decrease in local melt rate). Conversely, the first term in Eq. (7a) is positive, which says that the effect of increasing subglacial discharge on plume velocity causes an increase in local melt rate.

In the point source limit ($z \gg z_0$) of Eq. (7a), the second term tends to zero and the first term tends to 1/3. This is the region in which the effect of initial volume flux on plume temperature has been forgotten, and therefore $\dot{m} \propto Q_0^{1/3}$, with the exponent of 1/3 arising from the plume velocity. Away from the point source limit we must consider both plume velocity and temperature, and Eq. (7a) is best investigated numerically using the full model.

Taking $T_a = 3°C$ and $S_a = 33$ psu, we plot the value of Eq. (7a) as a function of z and Q_0 in Figs. 3a and 3c where $h = 300$ and 1000 m, respectively. We see that $0.30 < \gamma < 0.35$ for $z \gtrsim 8z_0$ and that γ is close to zero or negative for $z \lesssim z_0$, meaning that local melt rates decrease with increasing subglacial discharge. This occurs because, provided $T_a > T_0$, an increase in subglacial discharge decreases plume temperature and salinity, reducing thermal forcing $T - T_b$. This effect dominates over the change in plume velocity for $z \lesssim z_0$ (Figs. 3a,c). Note, however, that this statement is somewhat sensitive to plume initial conditions chosen at the grounding line; for $\Gamma_0 > 1$ local melt rates near the grounding line decrease more significantly with increasing subglacial discharge while for $\Gamma_0 < 1$ the effect is less significant. In general, however, it is a good approximation that local melt rates scale with $Q_0^{1/3}$ provided $z \gtrsim 8z_0$; otherwise, the exponent is smaller than 1/3 and may even be negative.

c. *Total submarine melt rates*

It is important to distinguish between local and total submarine melt rates. The latter is here defined by

$$\dot{M} = \int_0^h 2b\dot{m}\, dz, \tag{9}$$

and is the quantity measured by the heat flux gate estimates described in the introduction. We have discussed the character of $\dot{m}$ in the previous section; now we need also to consider plume radius b. Plume radius is insensitive to change in fjord temperature and salinity. Noting that

$$\frac{Q_0}{b}\frac{db}{dQ_0} = \frac{2}{5}\left(1 - \frac{z}{z + z_0}\right) \tag{10}$$

we see that $b \propto Q_0^{2/5}$ near the grounding line while b becomes independent of Q_0 in the point source limit. The discharge exponent of the integrand in Eq. (9) is obtained by summing Eq. (7a) and Eq. (10) and is plotted in Figs. 3b and 3d. For $z \lesssim z_0$, b dominates the exponent of the integrand while in the point source limit it does not contribute. Therefore, the presence of plume radius b in Eq. (9) rather effectively cancels out the parameter space in which the local melt rate exponent is small and so, except for very small z, the exponent of the integrand in Eq. (9) lies in the range 0.3–0.4 (Figs. 3b,d).

We seek last a value for the exponent in the relationship $\dot{M} \propto Q_0^{\gamma}$, plotted in Fig. 3e. This exponent is thus an integrated version of the exponents shown in Figs. 3b and 3d. For almost the full parameter space we have $0.30 < \gamma < 0.35$ (Fig. 3e). The value $\gamma < 0.3$ is only achieved when $h < z_0$. This occurs because the area of negative exponent seen in Fig. 3a becomes more dominant for smaller h. Since, to our knowledge, the vast majority of tidewater glaciers will satisfy $h > z_0$, it follows that the relationship $\dot{M} \propto Q_0^{1/3}$ will be a good approximation for total melt induced by half-conical plumes at tidewater glaciers.

We know from Eqs. (6a) and preceding discussion that in the point source limit ($z \gg z_0$) and at the fjord surface, $b \propto h$ and $\dot{m} \propto h^{-1/3}$, and thus $\dot{M} \propto h^{5/3}$. In sum, we can motivate a relationship between total submarine melt, forcings, and calving front height that reads

$$\dot{M} = A_1[1 + A_2(T_a - T_0)]Q_0^{1/3}h^{5/3}, \tag{11}$$

valid for $h > z_0$. Here A_1 and A_2 are two constants whose value can be obtained numerically by minimizing disagreement between Eq. (11) and the full model. For the ranges of h, T_a, and S_a indicated in Fig. 4, this yields $A_1 = 4.05 \times 10^{-6}\,\mathrm{m}^{1/3}\,\mathrm{s}^{-2/3}$ and $A_2 = 0.75\,(^\circ\mathrm{C})^{-1}$. Agreement of Eq. (11) with the full model is then excellent (Fig. 4) within the parameter range considered (maximum relative error 25%), suggesting that Eq. (11) is useful for estimating total melt without recourse to numerical integration of the full equations. Note that within the parameter range considered, h has the strongest influence on total melt [Eq. (11) and Fig. 4b], followed by T_a, Q_0, and then S_a (Figs. 4c, 4a, and 4d, respectively). Note also that Eq. (11) remains a good estimate even if we relax the assumption $\Gamma_0 = 1$; the maximum relative error is less than 33% for $\frac{1}{4} < \Gamma_0 < 30$.

We next consider a linearly stratified fjord, where plumes may not reach the fjord surface and the relationship between submarine melt and subglacial discharge is modified.

4. Linear stratification

a. Defining equations

We now consider linear stratification in temperature or salinity (or both). Continuing to neglect the melt feedback, Eqs. (1c) and (1d) may be rewritten (Morton et al. 1956)

$$\frac{d}{dz}\left(\frac{\pi}{2}b^2 u g'_T\right) = -\frac{\pi}{2}b^2 u N_T^2, \quad \text{and} \tag{12a}$$

$$\frac{d}{dz}\left(\frac{\pi}{2}b^2 u g'_S\right) = -\frac{\pi}{2}b^2 u N_S^2, \tag{12b}$$

where $g'_T = -g\beta_T(T_a - T)$ and $g'_S = g\beta_S(S_a - S)$ are the reduced gravity of the plume due to temperature and salinity, and $N_T^2 = g\beta_T dT_a/dz$ and $N_S^2 = -g\beta_S dS_a/dz$ are the constant squared buoyancy frequencies due to linear stratification in temperature and salinity. Since fjords in Greenland are warmer and saltier at depth, we have $dT_a/dz < 0$ and $dS_a/dz < 0$ and thus $N_T^2 < 0$ and $N_S^2 > 0$. Using the linear equation of state Eq. (4), we can combine Eqs. (12a) and (12b) into one equation for the evolution of plume buoyancy:

$$\frac{d}{dz}\left(\frac{\pi}{2}b^2 u g'\right) = -\frac{\pi}{2}b^2 u N^2, \tag{13}$$

where $g' = g'_T + g'_S$ and $N^2 = N_T^2 + N_S^2$. As previously noted, it is salinity that dominates density variation in proglacial fjords, and therefore N^2 is dominated by N_S^2. Equations (1a), (1b), and (13) are equivalent to the equations considered in Morton et al. (1956). We now consider the effect of stratification on plume dynamics and submarine melt rates in three cases.

b. Stratification in temperature but not salinity

As a limiting case we consider stratification in temperature but not salinity. Since ambient temperature has a very weak effect on plume dynamics and provided the stratification is not too strong [$|N_T^2|^{3/8} < (2\pi)^{-1/4}\alpha^{-1/2}(Q_0 g'_0)^{1/4}h^{-1}$, see below], we can approximately use the uniform stratification solution from section 3 for b and u to integrate Eq. (12a), obtaining

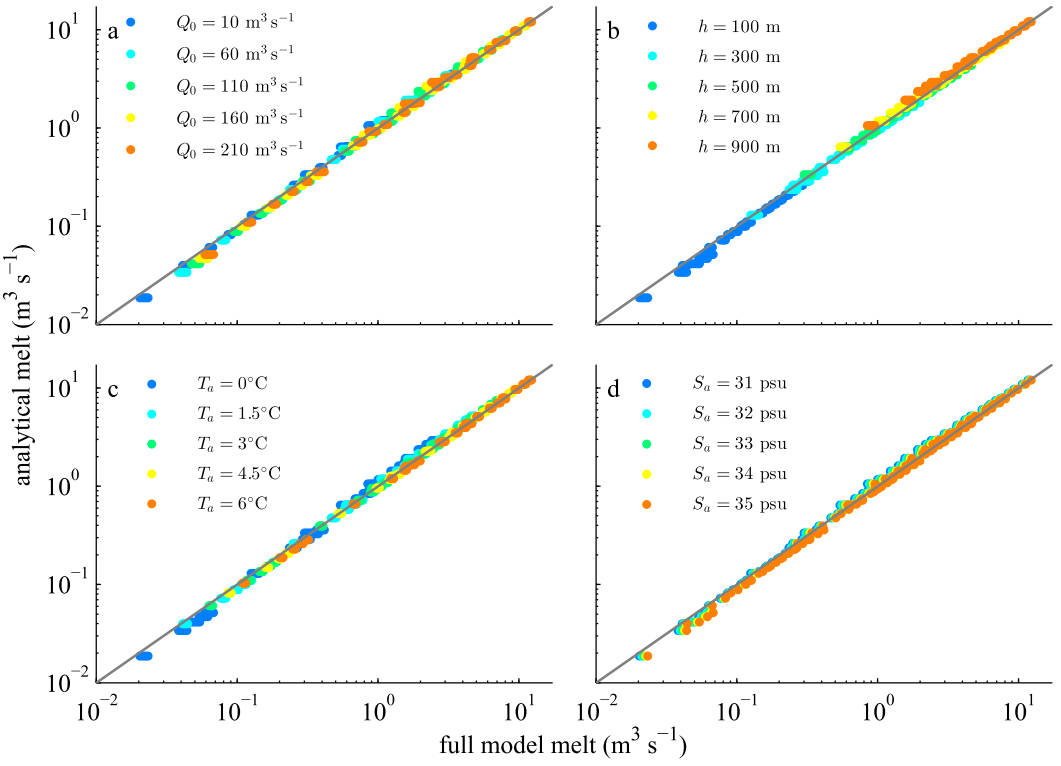

FIG. 4. Comparison of total melt from the full model (x axes) with total melt from Eq. (11) (y axes). Each data point represents a particular choice of parameters from the ranges indicated (thus, there are 750 data points on each plot). We distinguish data points by (a) subglacial discharge Q_0, (b) calving front height h, (c) fjord temperature T_a, and (d) fjord salinity S_a.

$$T_a - T = \frac{Q_0}{Q}(T_{a,0} - T_0) + \frac{3}{8}\frac{dT_a}{dz}\left\{z + z_0\left[1 - \left(\frac{z_0}{z + z_0}\right)^{5/3}\right]\right\}, \quad (14)$$

where $T_{a,0}$ is the ambient temperature at the grounding line. The first term on the right-hand side represents the uniform stratification solution, and the second term is the modification due to stratification. Note that with stratification in temperature, we no longer have $T_a - T \to 0$ in the point source limit (Fig. 5b) as in the uniform stratification case (Fig. 2).

Since local melt rates scale linearly with plume temperature, it follows from Eq. (14) that local and therefore total melt rates decrease linearly as $|dT_a/dz|$ increases (with ambient temperature at the grounding line held fixed). The second term on the right-hand side of Eq. (14) is an increasing but weak function of Q_0. Indeed, in the point source limit we obtain $T_a - T \approx (3/8)z dT_a/dz$, which is independent of Q_0. Therefore, the presence of stratification in temperature slightly increases the sensitivity of plume temperature to subglacial discharge, but temperature is independent of Q_0 in the point source limit. The exponent γ in the relationship $\dot{M} \propto Q_0^{\gamma}$ (Fig. 6a) therefore shows only minor differences to the uniform stratification case (Fig. 3e).

c. *Stratification in salinity but not temperature*

In this case we may no longer ignore the effect of stratification on plume dynamics, and the plume may become neutrally buoyant before the fjord surface (Fig. 5c; see also supplemental material). Consider a point source with buoyancy flux $B_0 = Q_0 g_0'$ in linear stratification $N^2 = N_S^2$. Scaling of plume properties with these parameters can be obtained by nondimensionalizing Eqs. (1a), (1b), and (13) following, for example, Morton et al. (1956) and Turner (1973). We obtain

$$b \propto B_0^{1/4}(N^2)^{-3/8}, \quad u \propto B_0^{1/4}(N^2)^{1/8}, \quad g' \propto B_0^{1/4}(N^2)^{5/8}, \quad \text{and} \quad z \propto B_0^{1/4}(N^2)^{-3/8}. \quad (15)$$

The characteristic length scale $B_0^{1/4}(N^2)^{-3/8}$ may be interpreted as the height through which the plume rises before stratification becomes important and may be

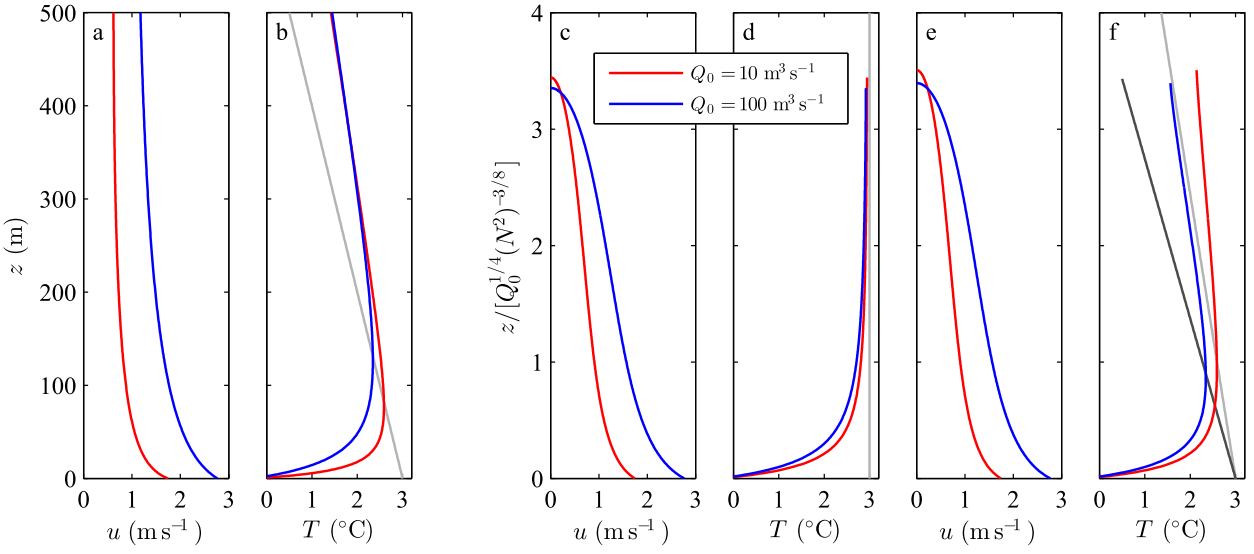

FIG. 5. Plume velocity and temperature in the linear stratification cases described in the text: (a), (b) $dT_a/dz = -0.005^\circ\mathrm{C\,m^{-1}}$ and $dS_a/dz = 0\ \mathrm{psu\,m^{-1}}$; (c),(d) $dT_a/dz = 0^\circ\mathrm{C\,m^{-1}}$ and $dS_a/dz = -0.005\ \mathrm{psu\,m^{-1}}$; and (e),(f) $dT_a/dz = -0.005^\circ\mathrm{C\,m^{-1}}$ and $dS_a/dz = -0.005\ \mathrm{psu\,m^{-1}}$. Note that in (c)–(f) we plot nondimensionalized z on the y axis. Gray lines show the ambient temperature; in (f) the plotting of nondimensional z on the y axis leads to two ambient temperature lines: the lighter gray applies for $Q_0 = 10\ \mathrm{m^3\,s^{-1}}$, the darker gray for $Q_0 = 100\ \mathrm{m^3\,s^{-1}}$. Ambient values at the grounding line are $T_{a,0} = 3^\circ\mathrm{C}$ and $S_{a,0} = 33$ psu.

motivated as the height over which a depth integral of the right-hand side of Eq. (13) becomes comparable to B_0. This scaling therefore represents a balance between dynamics dominated by the initial flux of buoyancy and dynamics dominated by the ambient stratification.

These scalings assume a point source for the plume located at $z = 0$; however, plumes at tidewater glaciers are initiated by finite sources. As motivated above, there is a region $z < z_1 = (2\pi)^{-1/4}\alpha^{-1/2}B_0^{1/4}(N^2)^{-3/8}$ (Morton 1959 and Fig. S1) in which a plume in a linear stratification behaves as if in a uniform stratification. Provided our finite source lies within this region (i.e., $z_0 < z_1$, which will be the case for glacial applications), we may trace back to a virtual point source, as in the uniform stratification case, and in particular identify the point source buoyancy flux B_0 with the finite source flux $Q_0 g_0'$ (Morton 1959; Hunt and Kaye 2001).

Beyond the region in which the uniform stratification solution is a good approximation, plume density approaches ambient values and the linear stratification solution departs from the uniform equivalent. The plume then undergoes buoyancy reversal at a height z_{br} and thereafter reaches a maximum height z_{mh} above the grounding line given by (e.g., Turner 1973; Hunt and Kaye 2001; see also supplemental material)

$$z_{\mathrm{br}} = 1.95(N^2)^{-3/8}\left(\frac{Q_0 g_0'}{2\pi\alpha^2}\right)^{1/4} - \frac{5}{6\alpha}\left(\frac{32\alpha Q_0^2}{5\pi^2 g_0'}\right)^{1/5}, \quad \text{and} \tag{16a}$$

$$z_{\mathrm{mh}} = 2.57(N^2)^{-3/8}\left(\frac{Q_0 g_0'}{2\pi\alpha^2}\right)^{1/4} - \frac{5}{6\alpha}\left(\frac{32\alpha Q_0^2}{5\pi^2 g_0'}\right)^{1/5}. \tag{16b}$$

Scaling of z_{br} and z_{mh} with Q_0 and N^2 is complicated by the finite source correction term appearing second in Eqs. (16). However, the first term dominates for parameter values relevant to tidewater glaciers, and characteristic plume heights scale approximately with $Q_0^{1/4}(N^2)^{-3/8}$.

Evolution of plume temperature contrast is given by Eq. (14) with $dT_a/dz = 0$. The response of plume temperature to change in subglacial discharge (Fig. 5d) is therefore similar to the uniform stratification case. It follows that in the point source limit $z \gg z_0$ (if the plume reaches this far) the response of melt rates to varying subglacial discharge is dominated by the effect on plume velocity.

Total submarine melt rate is given by

$$\dot{M} = \int_{z_0}^{z_{\mathrm{mh}}+z_0} 2b\dot{m}\,dz \quad \text{or} \quad \dot{M} = \int_{z_0}^{h+z_0} 2b\dot{m}\,dz, \tag{17}$$

where the first expression applies when the plume does not reach the surface ($z_{\mathrm{mh}} < h$) and the second when it does ($z_{\mathrm{mh}} > h$).

Assuming then that, under change in Q_0, local melt rates are controlled by plume velocity, it follows from Eqs. (15) that local melt rates would scale with $Q_0^{1/4}(N^2)^{1/8}$. The area of contact between the plume and

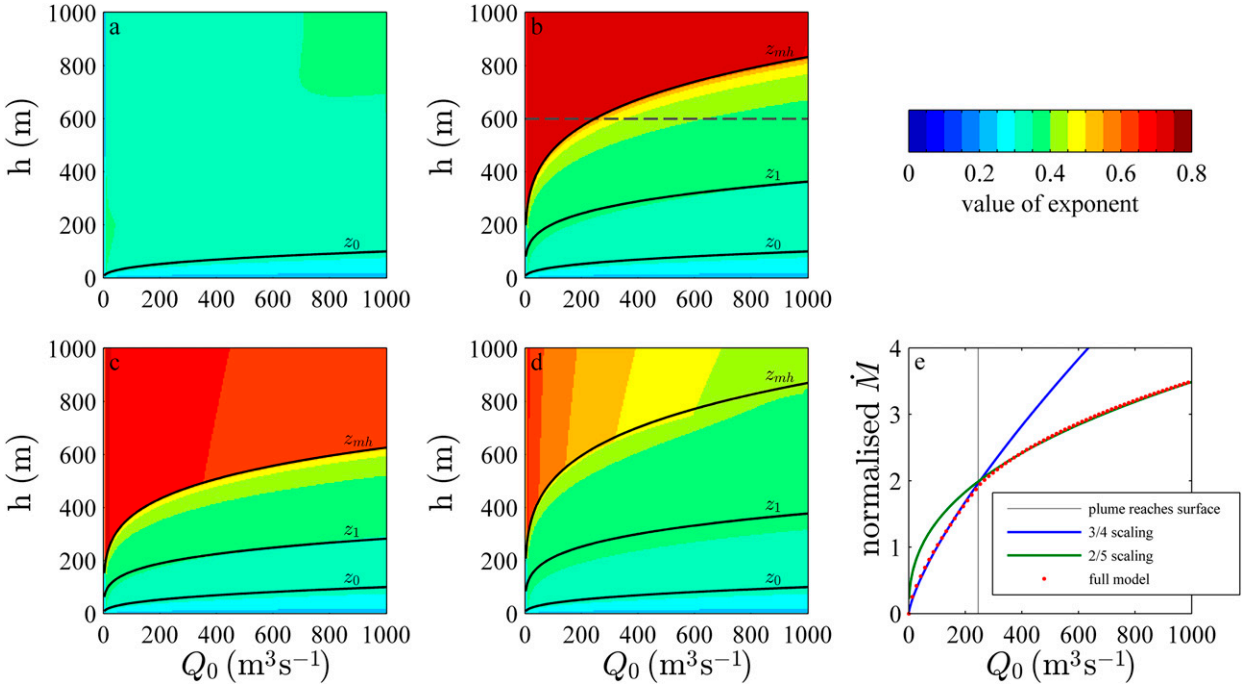

FIG. 6. Total melt rate discharge exponent (i.e., γ in the relationship $\dot{M} \propto Q_0^{\gamma}$) for linear stratifications: (a) $dT_a/dz = -0.005°\text{C m}^{-1}$ and unstratified in salinity, (b) $dS_a/dz = -0.005\,\text{psu m}^{-1}$ and unstratified in temperature, (c) $dT_a/dz = -0.005°\text{C m}^{-1}$ and $dS_a/dz = -0.01\,\text{psu m}^{-1}$, and (d) $dT_a/dz = -0.01°\text{C m}^{-1}$ and $dS_a/dz = -0.005\,\text{psu m}^{-1}$. (e) A specific example of the total melt rate discharge relationship for $h = 600$ m, which corresponds to the horizontal dashed line in (b). Solid black lines depict the three length scales that control melt rate exponent, as discussed in the text. Ambient values at the grounding line are $T_{a,0} = 3°\text{C}$ and $S_{a,0} = 33$ psu. Results are generated using the full model.

ice scales with $bz_{\text{mh}} \propto Q_0^{1/2}(N^2)^{-3/4}$ when the plume does not reach the surface and $bh \propto Q_0^{1/4}(N^2)^{-3/8}$ when it does, where we have neglected the point source correction.

The exponent in the relationship $\dot{M} \propto Q_0^{\gamma}$ (Fig. 6b) therefore varies depending on where calving front height h falls in relation to the three length scales $z_0 < z_1 < z_{\text{mh}}$. When $h < z_1$, plume dynamics are well approximated by the uniform stratification solution, and we may apply our results from section 3. For $z_1 < h < z_{\text{mh}}$ we lie in a transition regime where total melt rates combine the $Q_0^{1/2}(N^2)^{-1/4}$ velocity-induced scaling for total melt with the effect of Q_0 on plume temperature (the latter cannot be ignored because we do not satisfy $h \gg z_0$). Therefore, the total melt rate discharge exponent is reduced and ~2/5 provides an approximate value (Fig. 6e). Finally, when $h > z_{\text{mh}}$ we will also have $z \gg z_0$ for much of the calving front; therefore, local melt rates are controlled by plume velocity and total melt rates scale as $Q_0^{3/4}(N^2)^{-5/8}$ (Figs. 6b,e). Consideration of the point source correction results in only minor modifications to the exponents, discussed in the supplemental material.

d. Stratification in both temperature and salinity

While the preceding discussions provide interesting results that allow us to understand this last case, it is more usual to find stratification in salinity in concert with stratification in temperature. Plume width, velocity, and reduced gravity scale as in the previous section, with both N_S^2 and N_T^2 contributing to N^2 in this case. Plume temperature, however, is different. By combining Eqs. (12a) and (12b), evaluating the resulting expression at z_{mh} and noting the dominance of salinity in the equation of state, we obtain (supplemental material)

$$T_a - T \approx -(1+|\lambda|)\frac{dT_a/dz}{dS_a/dz}\frac{Q_0}{Q}(S_{a,0} - S_0)$$
$$\propto Q_0^{1/4}(N_T^2)(N_S^2)^{-3/8}, \tag{18}$$

where λ is some constant and $S_{a,0}$ is the ambient salinity at the grounding line.

We now compare this to previous sections. With stratification in salinity but not temperature, $T_a - T$ tends to 0 far from the grounding line (section 4c, Fig. 5d). With stratification in temperature but not salinity, $T_a - T$ became independent of Q_0 far from the grounding line (section 4b, Fig. 5b). The critical difference with stratification in both temperature and salinity is that at the furthest point from the grounding line, $T_a - T$ does not tend to 0 and retains sensitivity to

Q_0 [Eq. (18), Fig. 5f]. Therefore, when considering the effect of change in Q_0 on submarine melt, we must consider the effect on plume temperature. Equation (18) and Fig. 5f show that as Q_0 is increased, and at the point where the plume reaches its maximum height, plume temperature may be significantly decreased. This effect is less pronounced for small Q_0, small N_T^2 or large N_S^2 [Eq. (18)].

The total melt rate discharge exponent may therefore be substantially reduced relative to the case considered in section 4c. For $dT_a/dz = -0.005°\mathrm{C\,m^{-1}}$ and $dS_a/dz = -0.01\,\mathrm{psu\,m^{-1}}$ (Fig. 6c), the exponent is only slightly reduced. However, if we increase stratification in temperature and decrease stratification in salinity (Fig. 6d), the exponent may be reduced to ~½ and is only unaffected at low Q_0. Given the complexity of the relationship between total melt rate and subglacial discharge in the presence of stratification, it is not generally possible to obtain an equivalent of Eq. (11) when stratification is present.

5. Line plumes

For completeness, we now briefly consider the alternative geometry of line plumes. In the line plume case discharge is distributed uniformly across the glacier grounding line and is therefore appropriate for distributed subglacial drainage or low and very wide channels. The results are qualitatively similar to the half-conical geometry, and we therefore only highlight areas with interesting differences. The subglacial discharge Q_0 is regarded as a discharge per unit width of glacier. The plume is wedge shaped with the vertical side against the glacier and the inclined face in contact with the fjord (Fig. S2). Plume width $b(z)$ is taken as the thickness of the wedge at height z. Note that this is now the same model as considered in Jenkins (2011).

For a uniform stratification, an equivalent solution to Eqs. (6a)–(6c) is easily found (Linden et al. 1990; Jenkins 2011; Straneo and Cenedese 2015; see also supplemental material). The point source correction distance is given by $z_0 = (Q_0^2/\alpha^2 g_0')^{1/3}$. As in the half-conical case, the relative magnitude of z and z_0 determines the control on melt rate under change in subglacial discharge. In the point source limit $z \gg z_0$, change in melt due to change in subglacial discharge arises through the effect on velocity (note that this was the region considered by Jenkins 2011). For $z \sim z_0$ plume temperature must also be considered. Plots of the local melt rate exponent (Figs. 7a,b) show a similar form to the half-conical case, with an exponent of ⅓ (as found in Jenkins 2011) a good approximation for $z \gtrsim 15 z_0$. Note that for the half-conical case an exponent of ⅓ was good for $z \gtrsim 8 z_0$; the difference in length scales arises because the half-conical plume approaches ambient temperature more quickly than the line plume.

In contrast to the half-conical case, total melt rate per unit width of glacier is defined by

$$\dot{M} = \int_0^h \dot{m}\, dz. \tag{19}$$

The appearance of plume radius b in the half-conical equivalent definition [Eq. (9)] helped to ensure that the total melt rate exponent was close to ⅓ for $h > z_0$. In the line plume case, the differing integrand means that an exponent of ⅓ is only a good approximation for $h \gtrsim 70 z_0$ (Fig. 7c). Whether or not this provides a significant complication at real glaciers therefore depends on the calving front height and subglacial discharge. For example, at a calving front with $h = 500$ m, a total melt rate exponent of ⅓ is good for $Q_0 \lesssim 1\,\mathrm{m^2\,s^{-1}}$; for higher values of Q_0 the exponent will be reduced.

Finally, considering that melt approaches a constant value with depth, total melt rate is proportional to calving front height h. It follows that the line plume equivalent of Eq. (11) is

$$\dot{M} = A_1[1 + A_2(T_a - T_0)]Q_0^{1/3}h, \tag{20}$$

valid for $h \gtrsim 70 z_0$. Numerically, we obtain $A_1 = 1.56 \times 10^{-5}\,\mathrm{s^{-2/3}}$ and $A_2 = 0.84\ (°\mathrm{C})^{-1}$. Comparison of this equation and the full model is shown in Fig. S3 (maximum relative error is 13%).

In a linear stratification, line plume variables scale as $b \propto Q_0^{1/3}(N^2)^{-1/2}$, $u \propto Q_0^{1/3}$, and $g' \propto Q_0^{1/3}(N^2)^{1/2}$, while line plume characteristic heights z_{br} and z_{mh} scale as $Q_0^{1/3}(N^2)^{-1/2}$ (Wright and Wallace 1979; Bush and Woods 1999; see also supplemental material).

The character of submarine melting in a linear stratification is analogous to the half-conical case. With stratification in temperature but not salinity, uniform stratification results may be applied (Fig. 8a). With stratification in salinity but not temperature, and provided local melt rate follows plume velocity, we have total melt rates scaling with $Q_0^{2/3}(N^2)^{-1/2}$ when the plume does not reach the surface and $Q_0^{1/3}$ when it does (Fig. 8b). These exponents may, however, be reduced because of the effect of change in Q_0 on plume temperature. With stratification in both temperature and salinity, we expect a further reduction in exponents as decreasing plume temperature with increasing subglacial discharge reduces submarine melt rates (Figs. 8c,d).

6. Discussion

In the following we discuss first the relevance of characteristic plume heights to tidewater glaciers. We

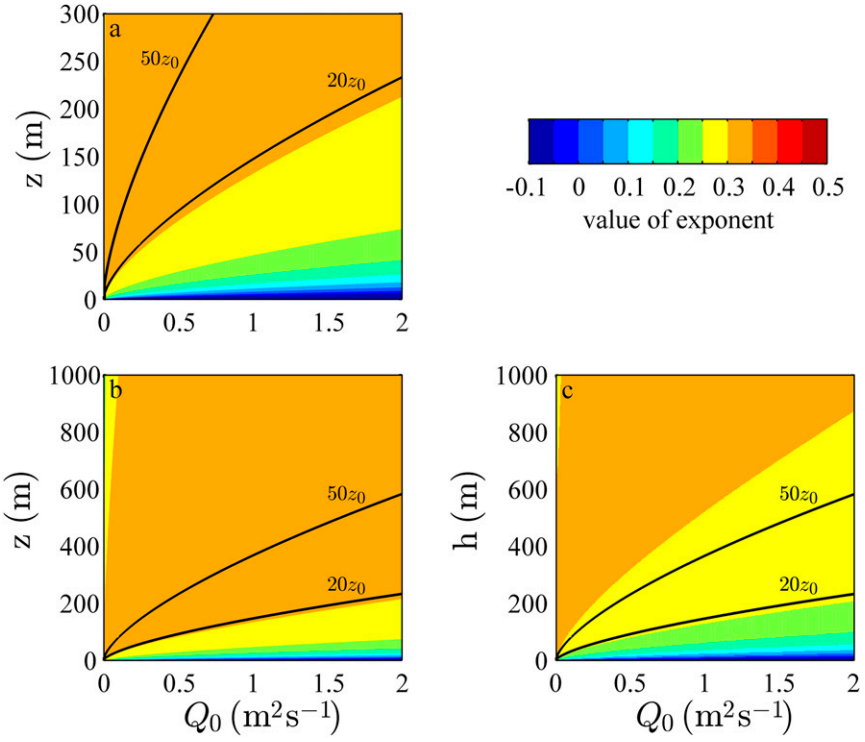

FIG. 7. Plots of local melt rate discharge exponent (i.e., γ in the relationship $\dot{m} \propto Q_0^{\gamma}$) for the line plume geometry: calving front height (a) $h = 300$ and (b) 1000 m. (c) Total melt rate discharge exponent (i.e., γ in the relationship $\dot{M} \propto Q_0^{\gamma}$) for the line plume geometry. Black lines show multiples of $z_0 = (Q_0^2/\alpha^2 g_0')^{1/3}$. Note that we do not consider the discharge exponent of $b\dot{m}$ in the line plume case, as the total melt integrand [Eq. (19)] does not contain b. Ambient values at the grounding line are $T_{a,0} = 3°C$ and $S_{a,0} = 33$ psu. Results are generated using the full model.

then consider the relationship between submarine melt rate and subglacial discharge and use our results to estimate variation in melt rates in recent decades and under projected atmospheric and oceanic warming. We finally discuss the implications for glacier dynamics.

In a linearly stratified fjord, the height of plume buoyancy reversal $z_{\rm br}$ and maximum plume rise $z_{\rm mh}$ scale approximately with subglacial discharge raised to the power 1/4 for a point source plume and 1/3 for a line source plume. We can use these scalings to comment on the visibility of a plume on the fjord surface. Consider a fjord of depth h. If the stratification and subglacial discharge are such that $z_{\rm br} > h$, the plume will be less dense than the ambient fjord water when it reaches the surface and will thus flow downfjord at the fjord surface, as is often observed in Greenland (e.g., Tedstone and Arnold 2012). If instead $z_{\rm mh} > h > z_{\rm br}$, the plume will reach the fjord surface adjacent to the glacier but will sink before flowing downfjord, likely undergoing some mixing as it sinks. The final possibility is $h > z_{\rm mh}$, in which case the plume does not reach the fjord surface and there may be no visible evidence of discharge emerging at the glacier grounding line.

The scalings can also be used to suggest the magnitude of subglacial discharge required for each of these transitions. To illustrate this, we consider an example from Store Glacier, West Greenland. Application of Eq. (16a) with $h = 500$ m, $N^2 \sim 2 \times 10^{-5}\,s^{-2}$, and $g_0' \sim 0.25\,m\,s^{-2}$ (from Fig. 2 in Chauché et al. 2014) suggests that $Q_0 \sim 140\,m^3\,s^{-1}$ is required before a plume from a single channel would flow away at the fjord surface, while Eq. (16b) suggests that $Q_0 \sim 40\,m^3\,s^{-1}$ is needed before the plume will first be visible at the fjord surface.

Considering now submarine melt, we find that no single scaling for melt with subglacial discharge and stratification can be applied universally. Rather, the appropriate scaling depends on a combination of the subglacial discharge, stratification, and calving front height. We give here a qualitative summary of our results. In a uniform stratification, local submarine melt rates close to the grounding line may decrease with increasing subglacial discharge when the resulting decrease in plume thermal forcing outweighs the increase in velocity. However, it remains the case that total submarine melt rate scales with subglacial discharge

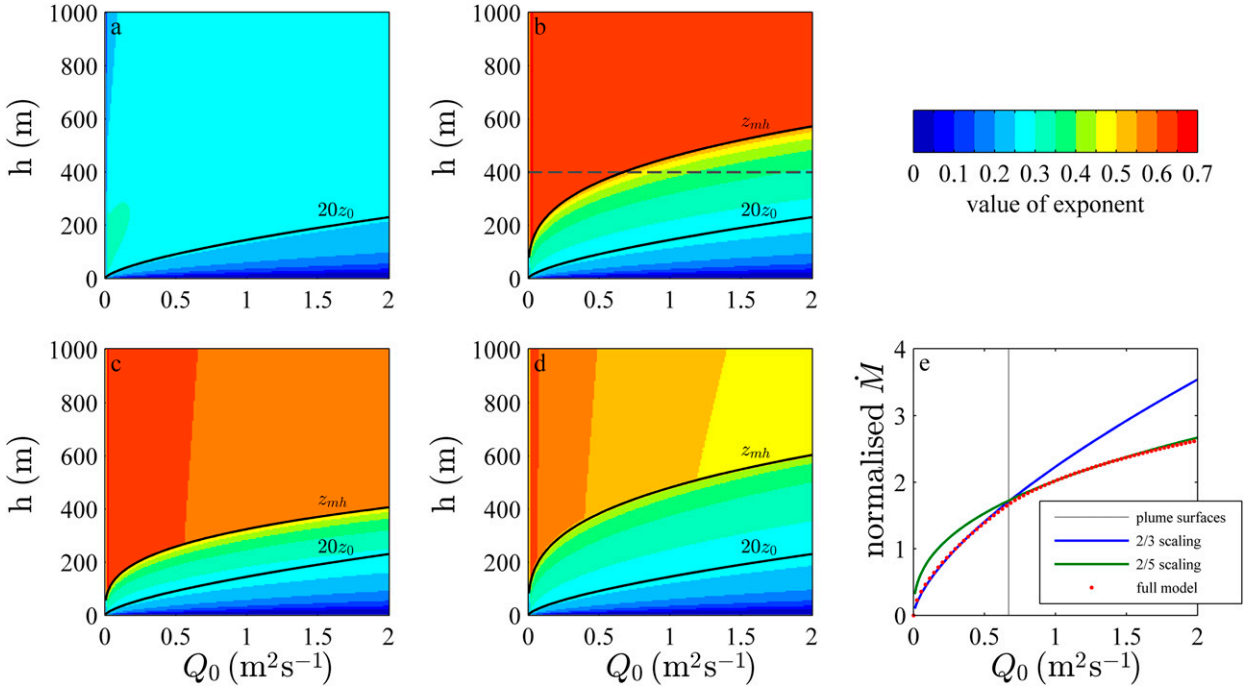

FIG. 8. Line plume equivalent of Fig. 6. Total melt rate discharge exponent (i.e., γ in the relationship $\dot{M} \propto Q_0^{\gamma}$) for linear stratifications: (a) $dT_a/dz = -0.005°\text{C m}^{-1}$ and unstratified in salinity, (b) $dS_a/dz = -0.005\,\text{psu m}^{-1}$ and unstratified in temperature, (c) $dT_a/dz = -0.005°\text{C m}^{-1}$ and $dS_a/dz = -0.01\,\text{psu m}^{-1}$, and (d) $dT_a/dz = -0.01°\text{C m}^{-1}$ and $dS_a/dz = -0.005\,\text{psu m}^{-1}$. (e) A specific example of the total melt rate discharge relationship for $h = 400$ m, which corresponds to the horizontal dashed line in (b).

raised to the power 1/3 regardless of plume geometry provided discharge does not exceed critical values as discussed in the results. Once linear stratification in salinity is introduced, the exponent may be as large as 3/4 (2/3) when a half-conical (line) plume does not reach the fjord surface. As subglacial discharge is increased and temperature stratification is introduced, this exponent is reduced.

Turning to previous work on the melt discharge exponent, Xu et al. (2012) and Sciascia et al. (2013) considered line plumes and found total melt rate exponents consistent with 1/3. Sciascia et al. (2013) had a two-layer stratification, but melt rates were dominated by the thicker lower layer that was unstratified. Xu et al. (2012) did not use a uniform stratification, but because they generated few data points when the plume did not reach the surface, they may not have been able to identify the 2/3 exponent predicted here.

Our half-conical plume results can be compared to three-dimensional numerical studies. In a uniform stratification, Kimura et al. (2014) found that a total melt rate exponent of 1/3 fitted their results until high initial plume velocities forced the plume away from the ice. With an observed stratification from in front of Store Glacier, Xu et al. (2013) suggested an exponent of 0.85 (0.5) at low (high) discharge. We believe the transition between these two values is similar to that which we observe in our results; total melt becomes less sensitive to subglacial discharge once the plume-ice contact area can no longer significantly increase. The slight differences in the exponent between Xu et al. (2013) and this paper might be explained by parameterization of turbulence in the numerical model (Slater et al. 2015) or the geometry of the plume source (Kimura et al. 2014). We therefore believe that our results regarding the melt discharge exponent are consistent with previous work and indeed can offer some explanation for the range of values reported.

Our study is most comparable to that of Jenkins (2011), which considered a line plume in the uniform stratification limit, finding a local melt rate discharge exponent of 1/3. As noted in section 2c, Jenkins (2011) focused on the region where buoyancy input from submarine melting is comparable to the initial buoyancy flux and was therefore able to neglect the region where plume temperature is not close to the ambient value. Our focus in this paper on the region in which the submarine melt feedback is negligible means we need to make explicit consideration of the evolution of plume temperature. For sufficiently small discharges, our results are in agreement with Jenkins (2011). However, for Greenland-relevant parameters, we

suggest that the local melt rate discharge exponent can be significantly reduced from 1/3 and may even be negative (Fig. 7a).

With the above understanding, we consider under what circumstances a certain exponent should apply. The larger exponents [2/3 for a distributed (line) input, 3/4 for a localized (point) input] apply for total melt rate when plumes do not reach the surface, although these exponents can be reduced by temperature stratification. It is probably necessary to solve the full equations to find an exact exponent. These exponents are likely relevant to glaciers terminating in deep fjords (e.g., Rink Isbrae) or glaciers with a distributed drainage system such that the discharge is split over many channels and is therefore less likely to reach the surface. An exponent of 1/3 applies for glaciers in weakly stratified or shallow fjords when plumes reach the surface (e.g., Svalbard or Alaska) or at large glaciers with high subglacial discharge. In these cases we derived simple expressions—Eqs. (11) and (20)—for estimating total submarine melt volume.

We can also use our scalings to assess the likely variation in submarine melting in recent decades and in the future. Assuming, for example, a warming of fjord water from 2° to 3°C (Holland et al. 2008), Eq. (11) suggests an increase in submarine melt of ~29%. Supposing runoff increased over the same period by ~25% (Hanna et al. 2011), a melt discharge exponent of 1/3 (3/4) gives an increase in submarine melting of 8% (18%). In combination, one can suggest that in recent decades submarine melt rates may have increased by up to ~50% in response to atmospheric and ocean warming. By the end of the century, under a doubling of subglacial discharge (Fettweis et al. 2013) and additional ocean warming of 2°C (Yin et al. 2011), we can estimate an 80% (140%) increase in submarine melting. Such estimates are of course simplistic in that they take no account of possible changes in fjord circulation or subglacial hydrology and rely on uncertain predictions of atmospheric and ocean warming.

When spatially averaged over a glacier terminus, predicted submarine melt rates (e.g., ~3 m day^{-1}; Slater et al. 2015) are generally much smaller than large Greenland tidewater glacier velocities (e.g., ~20 m day^{-1} at Helheim Glacier; Bevan et al. 2015). It should be noted that this study has focused on regions of the calving front affected by significant subglacial discharge; regions unaffected by subglacial discharge are still expected to melt (e.g., Sciascia et al. 2013) and may contribute to the spatially averaged melt rate. The above estimates nevertheless suggest that submarine melting would be unable to solely account for the recently observed retreat of such glaciers. If ocean forcing has been the primary driver of tidewater glacier behavior in recent decades, we therefore need to invoke a sensitive coupling between submarine melting and glacier dynamics. There is not yet a consensus in the literature on whether this coupling exists.

In a recent model of Store Glacier, Todd and Christoffersen (2014) found that terminus position was insensitive to an increase in submarine melt rate of up to 100%, an observation that they attributed to the particular bed and lateral topography at Store. At Helheim Glacier, Cook et al. (2014) found an order of magnitude increase in submarine melt was required to make the modeled glacier retreat. These studies therefore suggest that our estimated changes in submarine melting in recent decades would be unable to drive significant glacier retreat. In contrast, other studies (Weertman 1974; Nick et al. 2009; Enderlin et al. 2013) propose that glaciers with beds that deepen inland can respond dramatically to terminus perturbation through the marine ice sheet instability, and O'Leary and Christoffersen (2013) advocate a sensitive coupling between submarine melting and calving rate that may not be fully captured in models to date. Therefore, even with estimates of variation in melt rates in recent decades, the role of submarine melting in the dynamics of Greenland's tidewater glaciers remains ambiguous.

We note one final point regarding our results. The submarine melt rate parameterization Eqs. (2a)–(2c) should be used with caution, as it has thus far only been validated beneath an Antarctic ice shelf (Jenkins et al. 2010), and therefore, there is significant uncertainty in the value of the heat and salt transfer coefficients Γ_T and Γ_S. However, provided the form of the melt rate parameterization does not change [i.e., $\dot{m} \propto u(T - T_b)$], our scalings are unaffected by this uncertainty.

7. Conclusions

In this paper we have used buoyant plume theory to investigate the dynamics of proglacial plumes arising from the input of subglacial discharge at the grounding line of tidewater glaciers, focusing on the induced submarine melting of the calving front. In particular we have aimed to derive scalings for variation in submarine melt rates in terms of subglacial discharge, fjord properties, and calving front height.

We find that no simple relationship exists between submarine melt rate, subglacial discharge, and fjord stratification. We suggest that the relationship between subglacial discharge and submarine melt rate prevalent in the literature (i.e., submarine melt rate scales with subglacial discharge raised to the 1/3 power) is appropriate for local or total melt rates in a uniformly stratified fjord regardless of plume source geometry provided

discharge does not exceed a critical value. In these cases, it is possible to formulate simple equations for total melt induced [Eqs. (11), (20)]. However, once linear stratification is introduced, the total melt rate discharge exponent may be as large as 3/4 (2/3) for a point (line) source plume, though the exponent is complicated by stratification in temperature that may reduce the exponent somewhat. These higher exponents are likely representative for large glaciers terminating in deep water in Greenland where plumes are rarely seen, and where submarine melt rates could therefore be more sensitive to the magnitude of subglacial discharge than previously thought. Our findings are also able to explain the range of values of the exponent found in the literature.

We used our melt rate scalings to estimate that submarine melt rates may have increased by ~50% in recent decades, driven by a combination of atmospheric and ocean warming. Whether this is sufficient to explain the observed dynamic changes at tidewater glaciers in Greenland over the same time period remains uncertain; if it is, this would indicate a sensitive coupling between submarine melting and calving dynamics. Since submarine melting is likely to increase in response to predicted atmospheric and ocean warming, it is clear there is the potential for future dynamic response of tidewater glaciers to submarine melting and thus the need for further research into ice–ocean interaction in Greenland.

Acknowledgments. Donald Slater is supported by a NERC PhD studentship. Tom Cowton is supported by NERC Grant NE/K014609/1 awarded to Peter Nienow and Andrew Sole.

REFERENCES

Bartholomaus, T. C., C. F. Larsen, and S. O'Neel, 2013: Does calving matter? Evidence for significant submarine melt. *Earth Planet. Sci. Lett.*, **380**, 21–30, doi:10.1016/j.epsl.2013.08.014.

Bevan, S. L., A. Luckman, S. A. Khan, and T. Murray, 2015: Seasonal dynamic thinning at Helheim Glacier. *Earth Planet. Sci. Lett.*, **415**, 47–53, doi:10.1016/j.epsl.2015.01.031.

Bush, J. W. M., and A. W. Woods, 1999: Vortex generation by line plumes in a rotating stratified fluid. *J. Fluid Mech.*, **388**, 289–313, doi:10.1017/S0022112099004759.

Carroll, D., D. A. Sutherland, E. L. Shroyer, J. D. Nash, G. A. Catania, and L. A. Stearns, 2015: Modeling turbulent subglacial meltwater plumes: Implications for fjord-scale buoyancy-driven circulation. *J. Phys. Oceanogr.*, **45**, 2169–2185, doi:10.1175/JPO-D-15-0033.1.

Cenedese, C., and P. F. Linden, 2014: Entrainment in two coalescing axisymmetric turbulent plumes. *J. Fluid Mech.*, **752**, R2, doi:10.1017/jfm.2014.389.

Chauché, N., and Coauthors, 2014: Ice-ocean interaction and calving front morphology at two west Greenland tidewater outlet glaciers. *Cryosphere*, **8**, 1457–1468, doi:10.5194/tc-8-1457-2014.

Cook, S., I. C. Rutt, T. Murray, A. Luckman, T. Zwinger, N. Selmes, A. Goldsack, and T. D. James, 2014: Modelling environmental influences on calving at Helheim Glacier in eastern Greenland. *Cryosphere*, **8**, 827–841, doi:10.5194/tc-8-827-2014.

Cowton, T., D. Slater, A. Sole, D. Goldberg, and P. Nienow, 2015: Modeling the impact of glacial runoff on fjord circulation and submarine melt rate using a new subgrid-scale parameterization for glacial plumes. *J. Geophys. Res. Oceans*, **120**, 796–812, doi:10.1002/2014JC010324.

Enderlin, E. M., I. M. Howat, and A. Vieli, 2013: High sensitivity of tidewater outlet glacier dynamics to shape. *Cryosphere*, **7**, 1007–1015, doi:10.5194/tc-7-1007-2013.

——, ——, S. Jeong, M.-J. Noh, J. H. van Angelen, and M. R. van den Broeke, 2014: An improved mass budget for the Greenland ice sheet. *Geophys. Res. Lett.*, **41**, 866–872, doi:10.1002/2013GL059010.

Fettweis, X., B. Franco, M. Tedesco, J. H. van Angelen, J. T. M. Lenaerts, M. R. van den Broeke, and H. Gallee, 2013: Estimating the Greenland ice sheet surface mass balance contribution to future sea level rise using the regional atmospheric climate model mar. *Cryosphere*, **7**, 469–489, doi:10.5194/tc-7-469-2013.

Fofonoff, P., and R. C. Millard, 1983: Algorithms for computation of fundamental properties of seawater. UNESCO Tech. Papers in Marine Science 44, 53 pp. [Available online at http://unesdoc.unesco.org/images/0005/000598/059832eb.pdf.]

Hanna, E., and Coauthors, 2011: Greenland ice sheet surface mass balance 1870 to 2010 based on twentieth century reanalysis, and links with global climate forcing. *J. Geophys. Res.*, **116**, D24121, doi:10.1029/2011JD016387.

Holland, D. M., and A. Jenkins, 1999: Modeling thermodynamic ice-ocean interactions at the base of an ice shelf. *J. Phys. Oceanogr.*, **29**, 1787–1800, doi:10.1175/1520-0485(1999)029<1787:MTIOIA>2.0.CO;2.

——, R. H. Thomas, B. de Young, M. H. Ribergaard, and B. Lyberth, 2008: Acceleration of Jakobshavn Isbrae triggered by warm subsurface ocean waters. *Nat. Geosci.*, **1**, 659–664, doi:10.1038/ngeo316.

Hunt, G. R., and N. B. Kaye, 2001: Virtual origin correction for lazy turbulent plumes. *J. Fluid Mech.*, **435**, 377–396, doi:10.1017/S0022112001003871.

——, and ——, 2005: Lazy plumes. *J. Fluid Mech.*, **533**, 329–338, doi:10.1017/S002211200500457X.

Inall, M. E., T. Murray, F. R. Cottier, K. Scharrer, T. J. Boyd, K. J. Heywood, and S. L. Bevan, 2014: Oceanic heat delivery via Kangerdlugssuaq fjord to the south-east Greenland ice sheet. *J. Geophys. Res. Oceans*, **119**, 631–645, doi:10.1002/2013JC009295.

Jackson, R. H., F. Straneo, and D. A. Sutherland, 2014: Externally forced fluctuations in ocean temperature at Greenland glaciers in non-summer months. *Nat. Geosci.*, **7**, 503–508, doi:10.1038/ngeo2186.

Jenkins, A., 1991: A one-dimensional model of ice shelf-ocean interaction. *J. Geophys. Res.*, **96**, 20 671–20 677, doi:10.1029/91JC01842.

——, 2011: Convection-driven melting near the grounding lines of ice shelves and tidewater glaciers. *J. Phys. Oceanogr.*, **41**, 2279–2294, doi:10.1175/JPO-D-11-03.1.

——, K. W. Nicholls, and H. F. J. Corr, 2010: Observation and parameterization of ablation at the base of Ronne Ice Shelf, Antarctica. *J. Phys. Oceanogr.*, **40**, 2298–2312, doi:10.1175/2010JPO4317.1.

Jiskoot, H., D. Juhlin, H. St Pierre, and M. Citterio, 2012: Tidewater glacier fluctuations in central east Greenland coastal and fjord regions (1980s–2005). *Ann. Glaciol.*, **53**, 35–44, doi:10.3189/2012AoG60A030.

Kaye, N. B., 2008: Turbulent plumes in stratified environments: A review of recent work. *Atmos.–Ocean*, **46**, 433–441, doi:10.3137/ao.460404.

Kimura, S., P. R. Holland, A. Jenkins, and M. Piggot, 2014: The effect of meltwater plumes on the melting of a vertical glacier face. *J. Phys. Oceanogr.*, **44**, 3099–3117, doi:10.1175/JPO-D-13-0219.1.

Linden, P. F., G. F. Lane-Serff, and D. A. Smeed, 1990: Emptying filling boxes: the fluid mechanics of natural ventilation. *J. Fluid Mech.*, **212**, 309–335, doi:10.1017/S0022112090001987.

MacAyeal, D. R., 1985: Evolution of tidally triggered meltwater plumes below ice shelves. *Oceanology of the Antarctic Continental Shelf*, Antarctic Research Series, Vol. 43, Amer. Geophys. Union, 133–143.

Mernild, S. H., E. Hanna, J. C. Yde, J. Cappelen, and J. K. Malmros, 2014: Coastal Greenland air temperature extremes and trends 1890–2010: Annual and monthly analysis. *Int. J. Climatol.*, **34**, 1472–1487, doi:10.1002/joc.3777.

Moon, T., I. Joughin, B. Smith, and I. Howat, 2012: 21st-century evolution of Greenland outlet glacier velocities. *Science*, **336**, 576–578, doi:10.1126/science.1219985.

Mortensen, J., K. Lennert, J. Bendtsen, and S. Rysgaard, 2011: Heat sources for glacial melt in a sub-Arctic fjord (Godthåbsfjord) in contact with the Greenland Ice Sheet. *J. Geophys. Res.*, **116**, C01013, doi:10.1029/2010JC006528.

Morton, B. R., 1959: Forced plumes. *J. Fluid Mech.*, **5**, 151–163, doi:10.1017/S002211205900012X.

——, G. Taylor, and J. Turner, 1956: Turbulent gravitational convection from maintained and instantaneous sources. *Proc. Roy. Soc. London*, **234**, 1–23, doi:10.1098/rspa.1956.0011.

Motyka, R. J., W. P. Dryer, J. Amundson, M. Truffer, and M. Fahnestock, 2013: Rapid submarine melting driven by subglacial discharge, Leconte Glacier, Alaska. *Geophys. Res. Lett.*, **40**, 5153–5158, doi:10.1002/grl.51011.

Mugford, R. I., and J. A. Dowdeswell, 2011: Modeling glacial meltwater plume dynamics and sedimentation in high-latitude fjords. *J. Geophys. Res.*, **116**, F01023, doi:10.1029/2010JF001735.

Nick, F. M., A. Vieli, I. M. Howat, and I. Joughin, 2009: Large-scale changes in Greenland outlet glacier dynamics triggered at the terminus. *Nat. Geosci.*, **2**, 110–114, doi:10.1038/ngeo394.

O'Leary, M., 2011: Frontal processes on tidewater glaciers. Ph.D. thesis, University of Cambridge, 184 pp.

——, and P. Christoffersen, 2013: Calving on tidewater glaciers amplified by submarine frontal melting. *Cryosphere*, **7**, 119–128, doi:10.5194/tc-7-119-2013.

Rignot, E., M. Koppes, and I. Velicogna, 2010: Rapid submarine melting of the calving faces of West Greenland glaciers. *Nat. Geosci.*, **3**, 187–191, doi:10.1038/ngeo765.

——, I. Velicogna, M. R. van den Broeke, A. Monaghan, and J. T. M. Lenaerts, 2011: Acceleration of the contribution of the Greenland and Antarctic ice sheets to sea level rise. *Geophys. Res. Lett.*, **38**, L10504, doi:10.1029/2011GL047109.

——, I. Fenty, D. Menemenlis, and Y. Xu, 2012: Spreading of warm ocean waters around Greenland as a possible cause for glacier acceleration. *Ann. Glaciol.*, **53**, 257–266, doi:10.3189/2012AoG60A136.

Sciascia, R., F. Straneo, C. Cenedese, and P. Heimbach, 2013: Seasonal variability of submarine melt rate and circulation in an East Greenland fjord. *J. Geophys. Res. Oceans*, **118**, 2492–2506, doi:10.1002/jgrc.20142.

——, C. Cenedese, D. Nicoli, P. Heimbach, and F. Straneo, 2014: Impact of periodic intermediary flows on submarine melting of a Greenland glacier. *J. Geophys. Res. Oceans*, **119**, 7078–7098, doi:10.1002/2014JC009953.

Shepherd, A., and Coauthors, 2012: A reconciled estimate of ice-sheet mass balance. *Science*, **338**, 1183–1189, doi:10.1126/science.1228102.

Slater, D. A., P. W. Nienow, T. R. Cowton, D. N. Goldberg, and A. J. Sole, 2015: Effect of near-terminus subglacial hydrology on tidewater glacier submarine melt rates. *Geophys. Res. Lett.*, **42**, 2861–2868, doi:10.1002/2014GL062494.

Straneo, F., and C. Cenedese, 2015: The dynamics of Greenland's glacial fjords and their role in climate. *Annu. Rev. Mar. Sci.*, **7**, 89–112, doi:10.1146/annurev-marine-010213-135133.

——, G. S. Hamilton, D. A. Sutherland, L. A. Stearns, F. Davidson, M. O. Hammill, G. B. Stenson, and A. Rosing-Asvid, 2010: Rapid circulation of warm subtropical waters in a major glacial fjord in East Greenland. *Nat. Geosci.*, **3**, 182–186, doi:10.1038/ngeo764.

Sutherland, D. A., and F. Straneo, 2012: Estimating ocean heat transports and submarine melt rates in Sermilik Fjord, Greenland, using lowered acoustic Doppler current profiler (LADCP) velocity profiles. *Ann. Glaciol.*, **53**, 50–58, doi:10.3189/2012AoG60A050.

Tedstone, A. J., and N. S. Arnold, 2012: Automated remote sensing of sediment plumes for identification of runoff from the Greenland ice sheet. *J. Glaciol.*, **58**, 699–712, doi:10.3189/2012JoG11J204.

Todd, J., and P. Christoffersen, 2014: Are seasonal calving dynamics forced by buttressing from ice mélange or undercutting by melting? Outcomes from full-Stokes simulations of Store Glacier, West Greenland. *Cryosphere*, **8**, 2353–2365, doi:10.5194/tc-8-2353-2014.

Turner, J. S., 1973: *Buoyancy Effects in Fluids.* Cambridge University Press, 412 pp.

van den Broeke, M., and Coauthors, 2009: Partitioning recent Greenland mass loss. *Science*, **326**, 984–986, doi:10.1126/science.1178176.

Vaughan, D. G., and Coauthors, 2013: Observations: Cryosphere. *Climate Change 2013: The Physical Science Basis*, T. F. Stocker et al., Eds., Cambridge University Press, 317–382.

Weertman, J., 1974: Stability of the junction of an ice sheet and an ice shelf. *J. Glaciol.*, **13** (67), 3–11.

Wells, A. J., and M. G. Worster, 2008: A geophysical-scale model of vertical natural convection boundary layers. *J. Fluid Mech.*, **609**, 111–137, doi:10.1017/S0022112008002346.

Wright, S. J., and R. B. Wallace, 1979: Two-dimensional buoyant jets in a stratified fluid. *J. Hydraul. Div.*, **105**, 1393–1406.

Xu, Y., E. Rignot, D. Menemenlis, and M. Koppes, 2012: Numerical experiments on subaqueous melting of Greenland tidewater glaciers in response to ocean warming and enhanced subglacial discharge. *Ann. Glaciol.*, **53**, 229–234, doi:10.3189/2012AoG60A139.

——, ——, I. Fenty, D. Menemenlis, and M. M. Flexas, 2013: Subaqueous melting of store glacier, West Greenland from three-dimensional, high-resolution numerical modeling and ocean observations. *Geophys. Res. Lett.*, **40**, 4648–4653, doi:10.1002/grl.50825.

Yin, J., J. T. Overpeck, S. M. Griffies, A. Hu, J. L. Russell, and R. J. Stouffer, 2011: Different magnitudes of projected subsurface ocean warming around Greenland and Antarctica. *Nat. Geosci.*, **4**, 524–528, doi:10.1038/ngeo1189.